The Astrophysical Journal Supplement Series, 236:38 (15pp), 2018 June https://doi.org/10.3847/1538-4365/aabd3a


# FIT*spec*: A New Algorithm for the Automated Fit of Synthetic Stellar Spectra for OB Stars

Celia R. Fierro-Santillán[1], Janos Zsargó[2], Jaime Klapp[1,3], Santiago A. Díaz-Azuara[4], Anabel Arrieta[5], Lorena Arias[5], and Leonardo Di G. Sigalotti[6]

[1] ABACUS-Centro de Matemática Aplicada y Cómputo de Alto Rendimiento, Departamento de Matemáticas, Centro de Investigación y de Estudios Avanzados (Cinvestav-IPN), Carretera México-Toluca km. 38.5, La Marquesa, 52740 Ocoyoacac, Estado de México, Mexico
[2] Escuela Superior de Física y Matemáticas, Instituto Politécnico Nacional (IPN), Luis Enrique Erro S/N, San Pedro Zacatenco, 07738 Gustavo A. Madero, Ciudad de México, Mexico
[3] Departamento de Física, Instituto Nacional de Investigaciones Nucleares (ININ), Carretera México-Toluca km. 36.5, La Marquesa, 52750 Ocoyoacac, Estado de México, Mexico
[4] Instituto de Astronomía, Universidad Nacional Autónoma de México (UNAM), Avenida Universidad, 04510 Ciudad de México, Mexico
[5] Universidad Iberoamericana, Prolongación Paseo de la Reforma 880, Santa Fe, Contadero, 01219 Ciudad de México, Mexico
[6] Área de Física de Procesos Irreversibles, Departamento de Ciencias Básicas, Universidad Autónoma Metropolitana-Azcapotzalco (UAM-A), Av. San Pablo 180, 02200 Mexico City, Mexico

*Received 2017 October 27; revised 2018 March 27; accepted 2018 April 6; published 2018 June 1*

## Abstract

In this paper we describe the FIT*spec* code, a data mining tool for the automatic fitting of synthetic stellar spectra. The program uses a database of 27,000 CMFGEN models of stellar atmospheres arranged in a six-dimensional (6D) space, where each dimension corresponds to one model parameter. From these models a library of 2,835,000 synthetic spectra were generated covering the ultraviolet, optical, and infrared regions of the electromagnetic spectrum. Using FIT*spec* we adjust the effective temperature and the surface gravity. From the 6D array we also get the luminosity, the metallicity, and three parameters for the stellar wind: the terminal velocity ($v_\infty$), the $\beta$ exponent of the velocity law, and the clumping filling factor ($F_{\rm cl}$). Finally, the projected rotational velocity ($v \cdot \sin i$) can be obtained from the library of stellar spectra. Validation of the algorithm was performed by analyzing the spectra of a sample of eight O-type stars taken from the IACOB spectroscopic survey of Northern Galactic OB stars. The spectral lines used for the adjustment of the analyzed stars are reproduced with good accuracy. In particular, the effective temperatures calculated with the FIT*spec* are in good agreement with those derived from spectral type and other calibrations for the same stars. The stellar luminosities and projected rotational velocities are also in good agreement with previous quantitative spectroscopic analyses in the literature. An important advantage of FIT*spec* over traditional codes is that the time required for spectral analyses is reduced from months to a few hours.

*Key words:* astronomical databases: miscellaneous – stars: atmospheres – stars: fundamental parameters – stars: massive – stars: rotation

## 1. Introduction

Self-consistent analysis of spectral regions from the ultraviolet (UV) to the infrared (IR) radiation band has been made possible because of the large amount of publicly available data, combined with the existence of sophisticated stellar atmosphere codes such as CMFGEN (Hillier & Miller 1998), TLUSTY (Hubeny & Lanz 1995), FASTWIND (Santolaya-Rey et al. 1997; Puls et al. 2005), and the Postdam Wolf–Rayet (PoWR) code (Gräfener et al. 2002; Hamann & Gräfener 2003; Sander et al. 2015). As a result of this, significant advances have been made toward understanding the physical conditions prevailing in the atmospheres and winds of massive stars. For instance, Fullerton et al. (2000) showed that there were inconsistencies in the optical effective temperature scale in the early far-UV spectra when compared with the scale implied by the observed wind ionization. On the other hand, studies conducted by Martins et al. (2002) and Martins & Schaerer (2003) have shown that the neglect of line-blanketing in the models leads to a systematic overestimate of the effective temperature when derived from optical H and He lines. An improvement over these previous calibrations was reported by Martins et al. (2005), where a detailed treatment of non-LTE line-blanketing in the expanding atmospheres of massive stars was taken into account. After direct comparison to earlier calibrations of Vacca et al. (1996), they found effective temperature scales of dwarfs, giants, and supergiants that were lower from 2000 to 8000 K, with the reduction of temperature being the largest for the earliest spectral types and for supergiants. The luminosities were also reduced by 0.20–0.35 dex for dwarfs, about 0.25 dex for all giants, and by 0.25 to 0.35 dex for supergiants, with these reductions being almost independent of spectral type for the latter two cases. A treatment of iron group line-blanketing in non-LTE model atmospheres for Wolf–Rayet (WR) stars is described by Gräfener et al. (2002), where blanketing was found to affect their ionization structure and their emergent flux distribution. A temperature correction method for expanding atmospheres was also introduced by Hamann & Gräfener (2003), who showed that the method works quite well for Wolf–Rayet type models even in situations of strong non-LTE. A more recent analysis by Martins et al. (2015), using the CMFGEN code with line-blanketing included, found effective temperatures of Galactic O stars that were in good agreement with the FASTWIND values reported by Simón-Díaz & Herrero (2014) and Simón-Díaz et al. (2017). In addition, a set of O-type star models calculated with the PoWR code revealed that errors of a factor of two in the inferred spectroscopic mass can be expected when neglecting the contribution of line and

continuum transitions to the radiative acceleration in the photosphere (Sander et al. 2015). On the other hand, Crowther et al. (2002), Hillier et al. (2003), and Bouret et al. (2003) have simultaneously performed analyses of *FUSE*, *HST*, and optical spectra of O-type stars and were able to derive consistent effective temperatures using a wide variety of diagnostics.

A further important result was the recognition of the effects of wind inhomogeneities (i.e., clumping) on the spectral analyses of O-type stars. For instance, Crowther et al. (2002) and Hillier et al. (2003) were unable to reproduce the observed P v $\lambda\lambda$1118–1128 profiles when using mass-loss rates derived from the analysis of H$\alpha$ lines. The only way the P v and H$\alpha$ profile discrepancies could be resolved was by either assuming substantial clumping or using unrealistically low phosphorus abundances. Therefore, as a consequence of clumping, the mass-loss rates have been lowered by factors ranging from $\sim$3 to 10. Moreover, new observational clues for understanding macroturbulent broadening in massive O- and B-type stars have been provided by Simón-Díaz et al. (2017). They found that the whole O-type and B supergiant domain is dominated by massive stars ($M_{\rm ZAMS} \gtrsim 15\,M_{\odot}$), with a remarkable non-rotational line-broadening component, which has been suggested to be a spectroscopic signature of the presence of stellar oscillations in those stars. Recent spectral analyses of OB stars and the two WR binaries in the N206 superbubble of hot gas (in the Large Magellanic Cloud) show that the wind-momentum luminosity relation of the OB stars is consistent with expectations, and their HR diagram reveals a very large age spread (between 1 and 30 Myr), suggesting different episodes of star formation within N206 (Ramachandran et al. 2018).

Conducting the above investigations with the aid of any of the existing stellar atmosphere codes is by no means a simple task. Running these codes and performing reliable analyses and calibrations demands a lot of experience that unfortunately many researchers may have no time to acquire. On the other hand, for each interpolation, several models need to be run, which takes a long time. Thus, the program for fitting atmospheric parameters spends most of its time dealing with this. Therefore, it is desirable to optimize the calculation by developing databases of pre-calculated models, as well as the tools that are necessary for their use. Such databases will allow astronomers to save time and analyze stellar atmospheres with reasonable accuracy and without the need of running time-consuming simulations. Furthermore, these databases will also speed up the study of a large number of observed spectra that are still waiting for analysis.

The basic parameters of such databases of pre-calculated models are: the surface temperature ($T_{\rm eff}$), the stellar mass ($M$), and the surface chemical composition. However, an adequate analysis of massive stars must also take into account the parameters associated with the stellar wind, such as the terminal velocity ($v_{\infty}$), or the mass-loss rate ($\dot{M}$), and the line-clumping. If we take into account the variations of all necessary parameters, the number of pre-calculated models that is actually needed will increase exponentially. Therefore, production of such databases is only possible through the use of supercomputers.

At present, there are a few databases of synthetic stellar spectra available, but only with a few tens or hundreds of stellar models (see, for example, Hamann & Gräfener 2004; Fierro et al. 2015, or the POLLUX database (Palacios et al. 2010)). To improve on this we have developed a database with tens of thousands of stellar models (Zsargó et al. 2017), which we will release for public use in a short time. Since it is impossible to manually compare an observed spectrum with such an amount of models, it is imperative to develop appropriate tools that allow the automation of this process without compromising the quality of the fitting. With this in mind, we have created FIT*spec*, which is a program that searches in our database for the model that better fits the observed spectrum in the optical. This program uses Balmer lines to measure the surface gravity ($\log g$) and the line ratios He II/He I to estimate $T_{\rm eff}$. The paper is organized as follows. In Section 2, we describe the grid and the six-dimensional (6D) parameter space of the model database. In Section 3, we give a detailed description of the algorithm, and in Section 4, we test the algorithm by analyzing the spectra of a sample of eight O-type stars taken from the IACOB spectroscopic database of Northern Galactic OB stars. Finally, in Section 5 we summarize our main conclusions.

**Table 1**
Stellar Parameters

| Parameters in 6D space | Value |
|---|---|
| $T_{\rm eff}$ | from evolutive tracks[a] |
| $L$ | from evolutive tracks[a] |
| $Z$ | solar metallicity and solar metallicity enhanced by rotation from evolutive tracks[a] |
| $v_{\infty}$ | $2.1v_{\rm esc}$ |
| $\beta$ | 0.5, 0.8, 1.1, 1.4, 1.7, 2.1, 2.3 |
| $F_{\rm cl}$ | 0.05, 0.30, 0.60, 1.00 |
| **Other Parameters** | **Value** |
| $M$ | from evolutive tracks[a] |
| $R$ | from $M$ and $L$ |
| $\log g$ | from $M$ and $L$ |
| $v \sin i$ | from library of synthetic spectra |
| $\dot{M}$ | from evolutive tracks[a] |

**Note.**
[a] Ekström et al. (2012).

## 2. Model Database in a Six-dimensional Parameter Space

The stellar models are calculated using the more sophisticated and widely used non-LTE stellar atmosphere code CMFGEN (Hillier & Miller 1998). The code calculates the full spectrum and has been used successfully to model OB stars, WR stars, luminous blue variables, and even supernovae. It determines the temperature, the ionization structure, and the level populations for all elements in the stellar atmosphere and wind. It solves the radiative transfer equations in the co-moving frame in conjunction with the statistical and radiative equilibrium equations under the assumption of spherical symmetry. The hydrostatic structure can be computed below the sonic point, thereby allowing for the simultaneous treatment of spectral lines formed in the atmosphere, the stellar wind, and the transition region between the two. In particular, the code is well-suited for the study of massive OB stars with winds.

At present, our database contains 27,000 atmosphere models, arranged in a 6D space. When all parameter combinations are taken into account, we then expect to have 80,000 models. Each dimension in 6D space corresponds to one parameter of the model. In addition to the surface temperature ($T_{\rm eff}$), the luminosity ($L$), and the metallicity ($Z$)

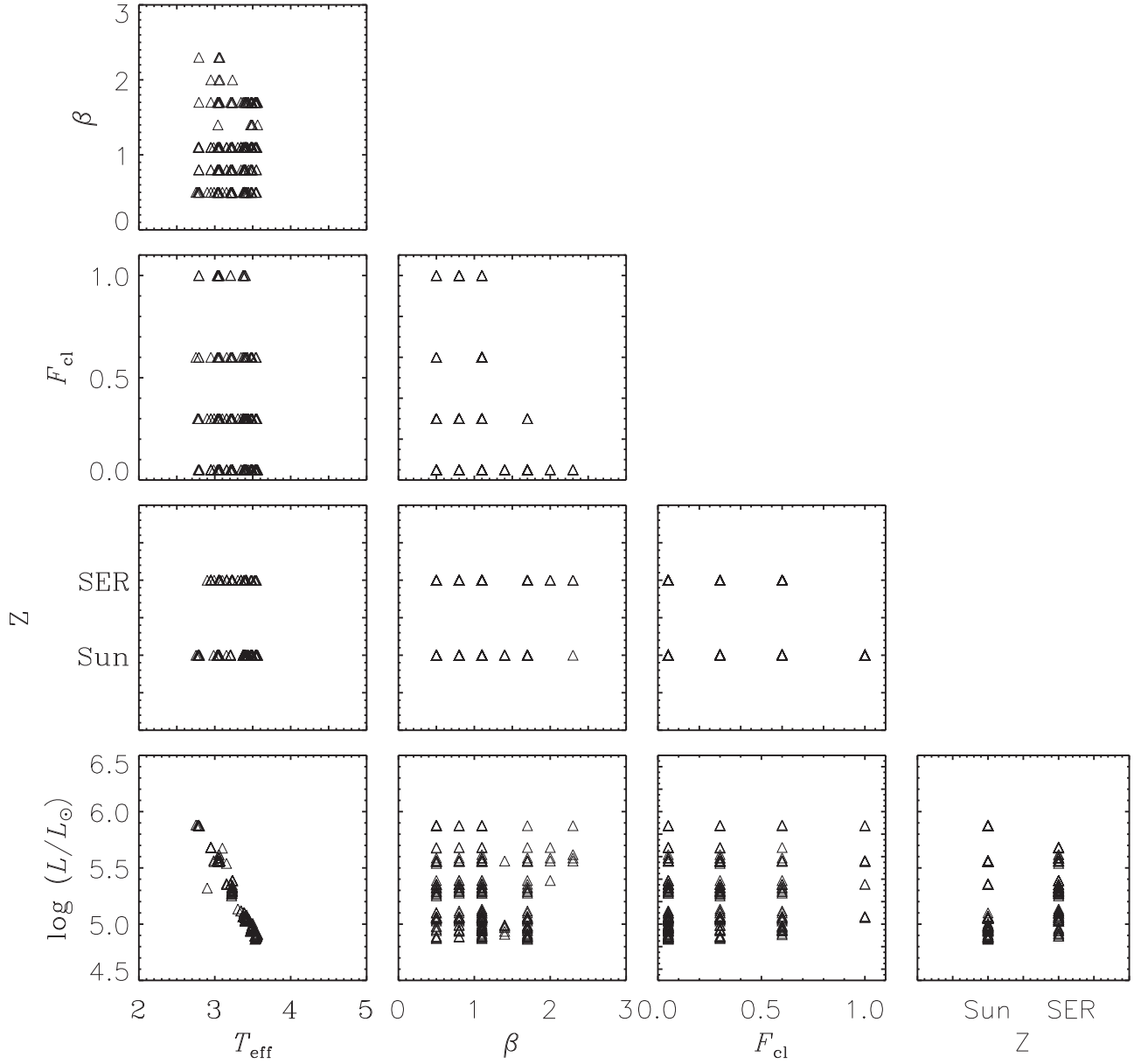


**Figure 1.** Distribution of the models with errors less than 50% in the six-dimensional (6D) parameter space for star HD 54662 of spectral type O7 V. In the first frame of the third row the legend Sun refers to solar metallicity, while SER refers to solar metallicity enhanced by rotation.

**Table 2**
Super Levels/Levels for the Different Ionization Stages Included in the Models

| Element | I | II | III | IV | V | VI | VII | VIII |
|---|---|---|---|---|---|---|---|---|
| H | 20/30 | 1/1 | … | … | … | … | … | … |
| He | 45/69 | 22/30 | 1/1 | … | … | … | … | … |
| C | … | 40/92 | 51/84 | 59/64 | 1/1 | … | … | … |
| N | … | 45/85 | 41/82 | 44/76 | 41/49 | 1/1 | … | … |
| O | … | 54/123 | 88/170 | 38/78 | 32/56 | 25/31 | 1/1 | … |
| Si | … | … | 33/33 | 22/33 | 1/1 | … | … | … |
| P | … | … | … | 30/90 | 16/62 | 1/1 | … | … |
| S | … | … | 24/44 | 51/142 | 31/98 | 28/58 | 1/1 | … |
| Fe | … | … | 104/1433 | 74/540 | 50/220 | 44/433 | 29/153 | 1/1 |

of the star, we consider three more parameters for the stellar wind, namely the terminal velocity ($v_\infty$), the $\beta$ exponent of the velocity law, and the clumping filling factor ($F_{\rm cl}$). Here, by $v_\infty$ we mean the velocity of the stellar wind at a large distance from the star. Outside the photosphere, we model the wind velocity as a function of the stellar radius using the $\beta$-type law

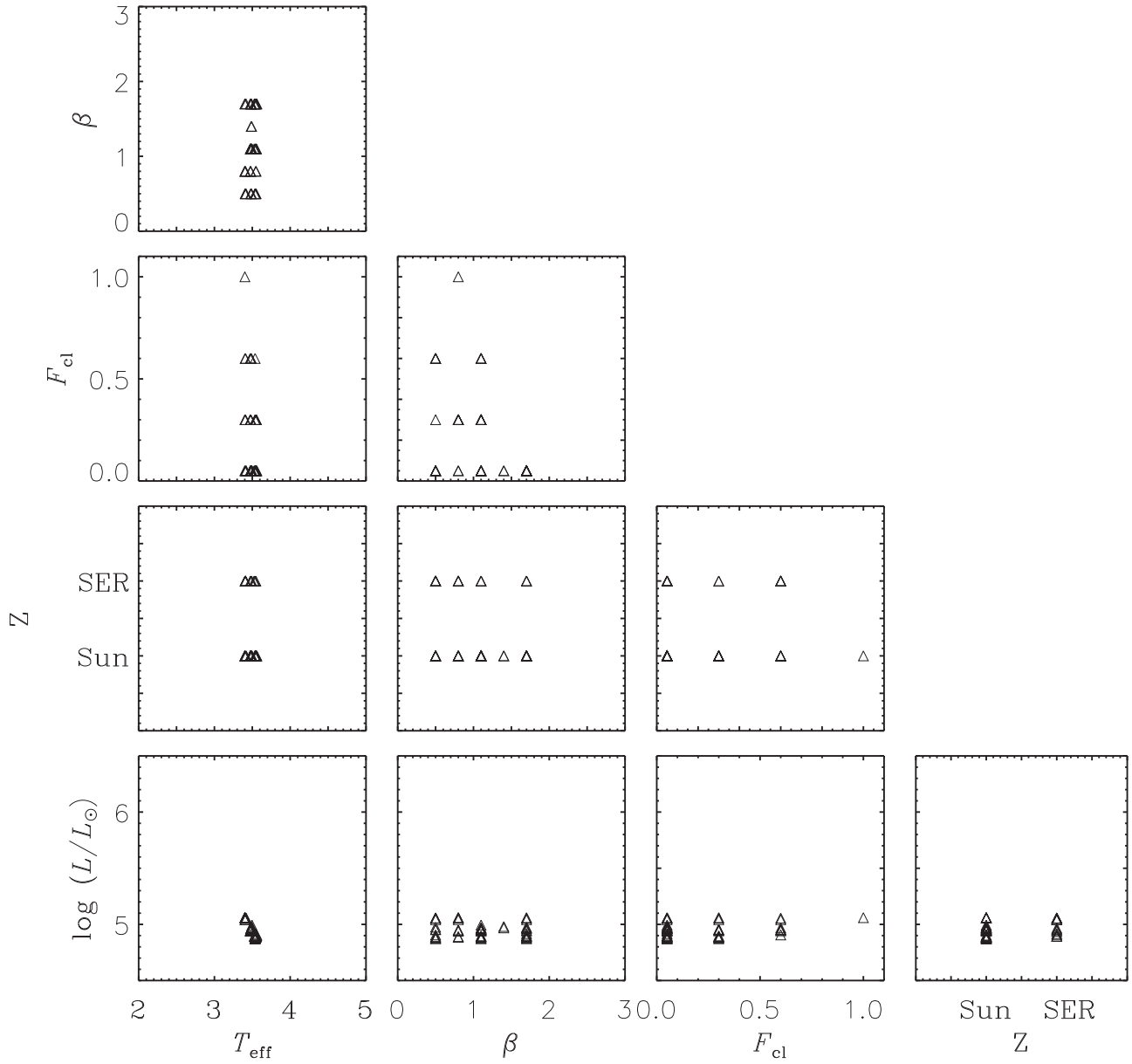


**Figure 2.** Distribution of the best-fit models (with errors less than 10%) in the six-dimensional (6D) parameter space for star HD 54662. In the first frame of the third row the legend Sun refers to solar metallicity, while SER refers to solar metallicity enhanced by rotation.

(Cassinelli & Olson 1979), i.e.,

$$v(r) = v_\infty \left(1 - \frac{r}{R_\star}\right)^\beta, \quad (1)$$

where the free parameter $\beta$ controls how the stellar wind is accelerated to reach the terminal velocity. Low values of $\beta$ (i.e., $\beta = 0.8$) indicate a fast wind acceleration, while high values (i.e., $\beta = 2.3$) indicate lower accelerations. Since the stellar wind is not necessarily homogeneous, we assume that it contains gas in the form of small clumps or condensations. The volume-filling factor $F_{\rm cl}$ is then the fraction of the total volume occupied by the gas clumps, while the space between them is assumed to be a vacuum. In addition, the mass-loss rate that is used for the models is taken from the evolutionary tracks of Ekström et al. (2012).

In Table 1 we list the values of the relevant model parameters. However, not all of them are truly free parameters. For instance, some of them are associated with other parameters (i.e., the mass-loss rate, $\dot{M}$, is completely determined when $T_{\rm eff}$, $\log g$, and $Z$ are known, while $R$ and $\log g$ depend on $M$ and $L$). The dependence of other parameters such as $\beta$ and $F_{\rm cl}$ has not been sufficiently explored, so they could be degenerate with other parameters. For each model, we calculate the synthetic spectra in the UV (900–3500 Å), optical (3500–7500 Å), and near-IR (7500–30000 Å) radiation bands. In order to facilitate comparison with the observations, the synthetic spectra are rotationally broadened using the program ROTIN3 (Hubeny & Lanz 1995), with rotational velocities between 10 and 350 km s$^{-1}$ separated by intervals of 10 km s$^{-1}$. These discrete values result in a library of 27,000 models × 3 bands × 35 values of the rotational velocity = 2,835,000 synthetic spectra. The main parameters of any model atmosphere are the luminosity ($L$) and the

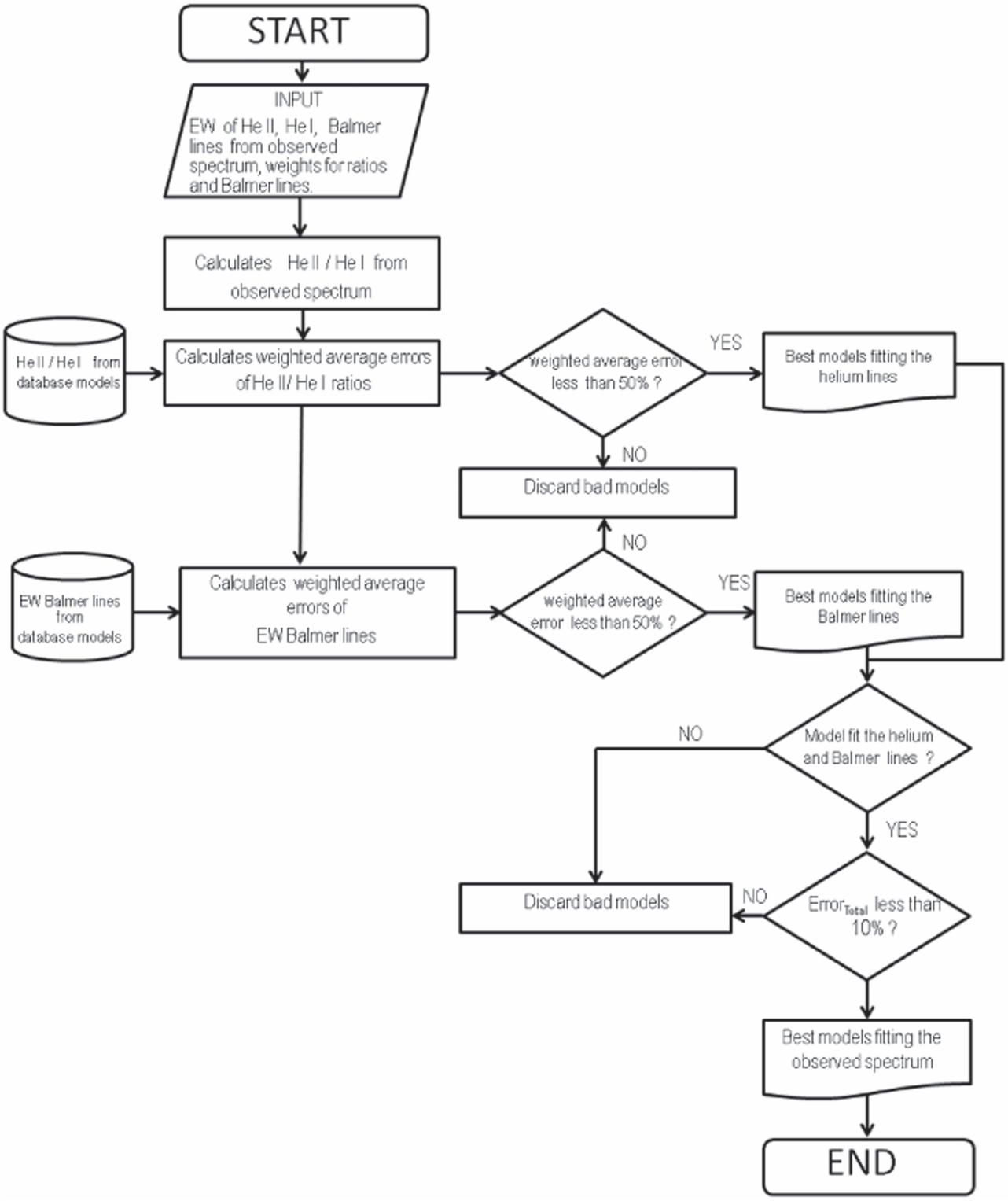


**Figure 3.** Flowchart showing the sequence of steps followed by the FIT*spec* algorithm.

effective temperature ($T_{\rm eff}$) from which we can determine the location of the star in the H–R diagram. As appropriate constraints to the input parameters, we use the evolutionary tracks of Ekström et al. (2012) calculated with solar metallicity ($Z = 0.014$) at the zero-age of the main sequence. Each point of a track corresponds to a star with specific values of $T_{\rm eff}$, luminosity ($L$), and stellar mass ($M$ ). We have calculated several models along each track at approximate discrete intervals of 2500 K in $T_{\rm eff}$. With this provision, the stellar radius, $R$, and the surface gravity, $\log g$, were calculated to determine the luminosity, $L$, and the stellar mass, $M$, corresponding to the track. The terminal velocities of the O-type stars in our sample are fitted by $v_\infty = 2.1 v_{\rm esc}$, where $v_{\rm esc}$ is the photospheric escape velocity. The chemical elements taken into account in our models are H, He, C, N, O, Si, P, S, and Fe. In particular, the values of the first five elements are taken from Ekström et al.

**Table 3**
Parameters of the Best-fit Models Found by FIT*spec*

| Star | $T_{\rm eff}$ (K) | $\log(\frac{L}{L_\odot})$ | $M$ ($M_\odot$) | $R$ ($R_\odot$) | $\log g$ (cm s$^{-2}$) | $Z$ | $\dot{M}$ ($M_\odot$ yr$^{-1}$) | $v_\infty$ (km s$^{-1}$) | $F_{\rm cl}$ | $\beta$ | $v \cdot \sin i$ (km s$^{-1}$) |
|---|---|---|---|---|---|---|---|---|---|---|---|
| HD 34078 | 33,580 ± 1000 | 4.66 ± 0.15 | 18.99 | 43.25 | 4.120 ± 0.12 | Sun[a] | $7.055 \times 10^{-9}$ | 2260 | 0.05 | 1.1 | 30 |
| HD 36512 | 31,280 ± 1000 | 4.40 ± 0.15 | 15.70 | 37.25 | 4.168 ± 0.12 | Sun[a] | $7.808 \times 10^{-9}$ | 2220 | 0.30 | 1.7 | 30 |
| HD 36879 | 32,220 ± 1000 | 5.25 ± 0.15 | 25.04 | 91.90 | 3.572 ± 0.12 | SER[b] | $2.063 \times 10^{-7}$ | 1770 | 0.30 | 0.8 | 180 |
| HD 37022 | 33,470 ± 1000 | 4.91 ± 0.15 | 21.66 | 58.37 | 3.913 ± 0.12 | SER[b] | $7.262 \times 10^{-8}$ | 2070 | 0.60 | 0.5 | 100 |
| HD 53975 | 35,030 ± 1000 | 4.63 ± 0.15 | 19.86 | 38.76 | 4.236 ± 0.12 | Sun[a] | $6.005 \times 10^{-9}$ | 2440 | 0.05 | 1.4 | 160 |
| HD 54662 | 35,500 ± 1000 | 4.90 ± 0.15 | 22.75 | 50.65 | 4.060 ± 0.12 | Sun[a] | $1.890 \times 10^{-8}$ | 2280 | 0.05 | 0.5 | 80 |
| HD 193322 | 32,460 ± 1000 | 4.74 ± 0.15 | 19.05 | 50.67 | 3.982 ± 0.12 | Sun[a] | $2.336 \times 10^{-8}$ | 2090 | 0.30 | 1.7 | 50 |
| HD 214680 | 32,980 ± 1000 | 4.66 ± 0.15 | 18.62 | 44.97 | 4.077 ± 0.12 | Sun[a] | $1.793 \times 10^{-8}$ | 2930 | 0.30 | 1.1 | 40 |

**Notes.**
[a] Solar metallicity: H, He, C, N, and, O are from the evolutive tracks of Ekström et al. (2012) and Si, P, S, and Fe are from Asplund et al. (2009).
[b] Solar metallicity enhanced by rotation: H, He, C, N, and, O are from the evolutive tracks of Ekström et al. (2012) and Si, P, S, and Fe are from Asplund et al. (2009).

(2012), while for consistency we take the solar metallicity reported by Asplund et al. (2009) for Si, P, S, and Fe in all models.

The code CMFGEN employs the concept of "super levels" for the atomic models, where levels of similar energy are grouped together and treated as a single level in the statistical equilibrium equations (see Hillier & Miller 1998, and references therein). The stellar models in this project include 28 explicit ions of different elements as a function of their $T_{\rm eff}$. Table 2 summarizes the levels and super levels that are included in the models. The atomic data references are given in the appendix of Herald & Bianchi (2004).

## 3. The FIT*spec* Algorithm

An experienced astronomer can make a qualitative fit by comparing by eye one or more models with the observed spectrum. However, this procedure becomes too cumbersome and time-consuming if hundreds of models must be compared. Also, when the number of models is too large, the objectivity can be easily compromised. FIT*spec* is a heuristic tool that mimics the procedure followed by an experienced astronomer to analyze observed stellar spectra. Due to the big size of the database, it is basically impossible to manually compare the observed spectra with the available models and find the best fit. For this purpose we have developed FIT*spec*, which was also designed to perform this task in a much shorter time compared to traditional fitting algorithms. The usual method to estimate $T_{\rm eff}$ in stellar atmospheres is to compare the equivalent widths (EW) of two lines of the same element in consecutive states of ionization. We have adopted four EW ratios of He II and He I lines to estimate $T_{\rm eff}$, namely

$$\frac{\mathrm{EW(He\ II\ }\lambda4541)}{\mathrm{EW(He\ I\ }\lambda4471)}, \tag{2a}$$

$$\frac{\mathrm{EW(He\ II\ }\lambda4200)}{\mathrm{EW(He\ I\ }\lambda4026)}, \tag{2b}$$

$$\frac{\mathrm{EW(He\ II\ }\lambda4200)}{\mathrm{EW(He\ I\ }\lambda4144)}, \tag{2c}$$

$$\frac{\mathrm{EW(He\ II\ }\lambda4541)}{\mathrm{EW(He\ I\ }\lambda4387)}. \tag{2d}$$

For comparison, Walborn & Fitzpatrick (1990) used the ratios 2(a) and (b) to classify O3-B0 main-sequence stars, while the ratios 2(c) and (d) were suitable only for the classification of the later types in the same range. In contrast, we have recorded these ratios for all models in our database. To use FIT*spec*, the user must provide the observed EW of He II $\lambda\lambda$ 4541, 4200; He I $\lambda\lambda$4471, 4387, 4144; and He I+He II $\lambda\lambda$ 4026 as input data. These values can be easily measured by any astronomical software as, for example, IRAF.[7] The algorithm then calculates the EW ratios for the observed lines and compares them with those for the models in the database.

Under the assumption that the best-fit model is the one that accurately reproduces the ratios for the observed spectrum, we can calculate the differences between the observed ratios and those pertaining to each model in terms of the relative error

$$\mathrm{Error}\left(\frac{\mathrm{He\ II}}{\mathrm{He\ I}}\right) = \frac{\left(\frac{\mathrm{He\ II}}{\mathrm{He\ I}}\right)_{\rm obs} - \left(\frac{\mathrm{He\ II}}{\mathrm{He\ I}}\right)_{\rm mod}}{\left(\frac{\mathrm{He\ II}}{\mathrm{He\ I}}\right)_{\rm obs}}, \tag{3}$$

where $(\mathrm{He\ II/He\ I})_{\rm obs}$ is any of the ratios calculated from the observed spectrum and $(\mathrm{He\ II/He\ I})_{\rm mod}$ is the corresponding ratio for a model. The metric defined by Equation (3) provides a good measure of the difference between models and observations.

FIT*spec* then calculates a weighted average of the errors in the four ratios considered. The weight of each ratio is an input parameter and must be provided by the user. The program was designed to find all models with average errors less than 50%, to save the description of these models in an output file, and to produce a graphical output to visualize the location of the models in the 6D parameter space (see Figure 1). The next step consists of estimating the surface gravity, $\log g$. For this purpose the EWs of the H I Balmer lines are used. The errors in the EWs of the six Balmer lines ($\lambda\lambda$3835, 3889, 3970, 4102, 4341, 4861) are then calculated, which are finally used to estimate the $\log g$ of the star. As for the spectral type–effective temperature (SpT–$T_{\rm eff}$) calibration, these errors are calculated using the metric

$$\mathrm{Error_{EW}} = \frac{\mathrm{EW_{obs} - EW_{mod}}}{\mathrm{EW_{obs}}}, \tag{4}$$

[7] IRAF is written and supported by the National Optical Astronomy Observatories (NOAO) in Tucson, Arizona. NOAO is operated by the Association of Universities for Research in Astronomy (AURA), Inc. under cooperative agreement with the National Science Foundation (NSF).

**Table 4**
Comparison of Parameters Found by FIT*spec* with the Results of Previous Calibrations

| Star | SpT | $T_{\rm eff}$ (K) FIT*spec* | $T_{\rm eff}$ (K) SpT | $T_{\rm eff}$ (K) other | $\log g$ (cm s$^{-2}$) FIT*spec* | $\log g$ (cm s$^{-2}$) SpT | $\log g$ (cm s$^{-2}$) other | $\log(\frac{L}{L_\odot})$ FIT*spec* | $\log(\frac{L}{L_\odot})$ SpT | $v \cdot \sin i$ (km s$^{-1}$) FIT*spec* | $v \cdot \sin i$ (km s$^{-1}$) other |
|---|---|---|---|---|---|---|---|---|---|---|---|
| HD 34078 | O9.5V | 33,580 ± 1000 | 30,488 ± 1000 | 33,000[a]<br>33,900 ± 1700[b]<br>36,500 ± 1000[c] | 4.120 ± 0.12 | 3.92 | 4.0 ± 0.15[a]<br>3.980[b]<br>4.05[c] | 4.66 ± 0.15 | 4.62 ± 0.15 | 30 | 25[a]<br>17[b]<br>40[c]<br>13[d]<br>27[e] |
| HD 36512 | O9.7V | 31,280 ± 1000 | 30,000[f] | 32,500[a]<br>33,900 ± 1700[b]<br>33,400 ± 200[g] | 4.168 ± 0.12 | 3.92[f] | 4.0 ± 0.15[a]<br>4.210[b]<br>4.30 ± 0.05[g]<br>4.13 [e] | 4.40 ± 0.15 | 4.58[f] | 30 | 20[a]<br>15[b]<br>20 ± 2[g]<br>15[d] |
| HD 36879 | O7V | 32,220 ± 1000 | 35,531 ± 1000 | 36,500[a] | 3.572 ± 0.12 | 3.92 | 3.75 ± 0.15[a] | 5.25 ± 0.15 | 5.10 ± 0.15 | 180 | 200[a]<br>219[d]<br>200[e] |
| HD 37022 | O7V | 33,470 ± 1000 | 35,531 ± 1000 | 38,900 ± 1700[b] | 3.913 ± 0.12 | 3.92 | 4.170[b] | 4.91 ± 0.15 | 5.10 ± 0.15 | 100 | 26[b]<br>98[e]<br>26[d] |
| HD 53975 | O7.5V | 35,030 ± 1000 | 34,419 ± 1000 | 35,500 ± 1900[b]<br>36,300[h] | 4.236 ± 0.12 | 3.92 | 3.590[b] | 4.63 ± 0.15 | 5.00 ± 0.15 | 160 | 186[b]<br>163[i]<br>180[d]<br>147[e] |
| HD 54662 | O7V | 35,500 ± 1000 | 35,531 ± 1000 | | 4.060 ± 0.12 | 3.92 | | 4.90 ± 0.15 | 5.10 ± 0.15 | 80 | 70[e] |
| HD 193322 | O9V | 32,460 ± 1000 | 31,524 ± 1000 | | 3.982 ± 0.12 | 3.92 | | 4.74 ± 0.15 | 4.72 ± 0.15 | 50 | 94[e]<br>41[d] |
| HD 214680 | O9V | 32,980 ± 1000 | 31,524 ± 1000 | 35,000[a]<br>35,500 ± 1900[b]<br>37,500 ± 1000[c] | 4.077 ± 0.12 | 3.92 | 4.05 ± 0.15[a]<br>3.920[b]<br>4.0[c] | 4.66 ± 0.15 | 4.72 ± 0.15 | 40 | 15[a]<br>16[b]<br>50[c]<br>32[e]<br>16[d] |

**Notes.**
[a] Martins et al. (2015).
[b] Simón-Díaz et al. (2017).
[c] Villamariz & Herrero (2002).
[d] Simón-Díaz & Herrero (2014).
[e] Conti & Ebbets (1977).
[f] Extrapolated using the data of Table 1 of Martins et al. (2005).
[g] Nieva (2013).
[h] Sybesma & De Loore (1982).
[i] Oliveira & Hébrard (2006).

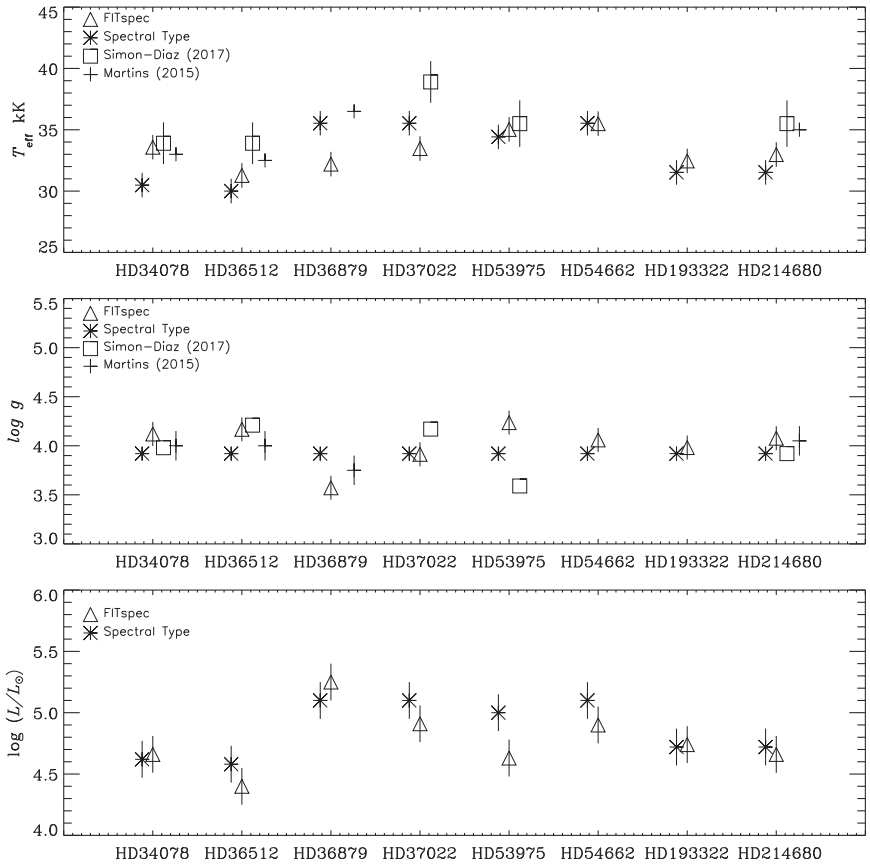


**Figure 4.** (Top panel) Effective temperatures found by FIT*spec* (triangles) compared to the corresponding values obtained from the spectral type (asterisks) and the adjustments of Martins et al. (2015; plus signs) and Simón-Díaz et al. (2017; squares). The largest error bar corresponds to a temperature interval of 1.9 kK, while the shortest one corresponds to a length of 1 kK. (Middle panel) Surface gravity found by FIT*spec* (triangles) compared to the corresponding values obtained from spectral type (asterisks) and the adjustments of Martins et al. (2015; plus signs) and Simón-Díaz et al. (2017; squares). The lengths of the error bars are 0.12 dex for the FIT*spec* data and 0.15 dex for the calibrations of Martins et al. (2015). (Bottom panel) Logarithm of the luminosity found by FIT*spec* (triangles) compared to the corresponding values obtained from the spectral type (asterisks). All error bars correspond to 0.15 dex.

where $\mathrm{Error_{EW}}$ indicates how different a model and the observation are for a specific line. FIT*spec* also calculates the weighted averages of the relative errors in the EWs of the Balmer lines where the weights must be provided by the user. The algorithm first finds out the models that are within an error of 50% and then picks those models that have both Error(He II/He I) and $\mathrm{Error_{EW}}$ less than 50%. The total error is calculated according to

$$\mathrm{Error_{tot}} = \sqrt{(\mathrm{Error_{EW}})^2 + \left[\mathrm{Error}\left(\frac{\mathrm{He\ II}}{\mathrm{He\ I}}\right)\right]^2}. \quad (5)$$

Finally, the program sorts the errors from the lowest to the highest values of $\mathrm{Error_{tot}}$ and generates a file containing only those models whose total error is less than 10% (see Figure 2). The sequence of steps followed by FIT*spec* is shown as a flowchart in Figure 3.

## 4. Results and Discussion

Validation of FIT*spec* is made by testing the algorithm for a sample of eight O-type main-sequence stars. These stars were chosen on the basis of having known available observational data and spectral classification in the IACOB database (Simón-Díaz et al. 2011). In addition, they are located in a region of the H–R diagram where our database has the highest density of models. Table 3 lists the stellar parameters as obtained from the best-fitted models as found by FIT*spec* for each selected star in our sample. Uncertainties in the effective temperature and luminosity are 1 kK and 0.15 dex, respectively, for all models in the sample. These uncertainties were estimated from the models themselves. The errors in $T_{\rm eff}$ take into account the models that reasonably fit the EWs of the He I and He II lines in a global way, while the errors in $L$ include the models that reasonably fit the EWs of the Balmer lines in a global way. In addition, the first and second columns of Table 4 list the selected stars and their spectral types, respectively, while the next eight columns compare their effective temperatures, surface gravities, and luminosities (also listed in Table 3) with the corresponding values from spectral type calibrations and other spectral analyses reported in the literature. Finally, the last two columns in Table 4 compare the projected rotational velocities as found by FIT*spec* with the corresponding values obtained from several other spectral calibrations, as indicated by the references listed in the footnote of Table 4.

In passing, we note that star HD 54662 is a peculiar object. Some authors have treated it as if it were a single star (Markova et al. 2004; Krticka & Kubat 2010), although there is enough evidence that it is actually a binary star (Fullerton 1990; Sana et al. 2014; Mossoux et al. 2018). However, in this work HD 54662 was also taken as a single star because the spectrum extracted from the IACOB database shows no evidence of binarity. The corner plots of Figure 1 show the distribution in

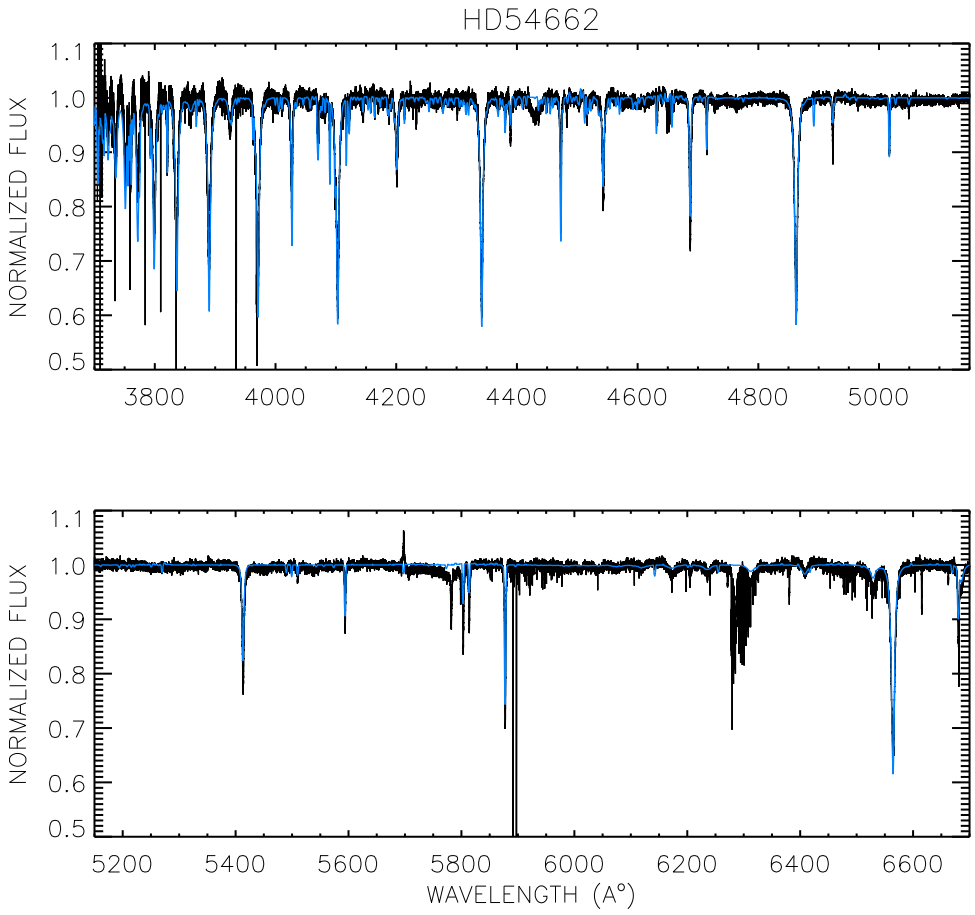


**Figure 5.** Comparison of the observed spectrum (black line) with that of the best-fit model (blue line) for the star HD 54662.

the 6D space of the models with relative errors less than 50% in the He II/He I ratios for star HD 54662 of spectral type O7 V, while Figure 2 shows the distribution of the models when $\text{Error}_{\text{tot}} \lesssim 10\%$ for the same star. When only the temperature criterion is considered, the models span a finite range of values of the parameter space. That is, for prescribed values of the metallicity, filling factor, and $\beta$ exponent of the velocity law, the effective temperature and luminosity of the star can have different values over a finite range. However, when the more stringent criterion $\text{Error}_{\text{tot}} \lesssim 10\%$ is applied, the effective temperature and luminosity, vary over very narrow intervals of values with varying metallicity, filling factor, and $\beta$ exponent, as we may see from the first column and last row of frames in Figure 2.

The effective temperatures $T_{\text{eff}}$ from spectral type were calculated using the calibrations of Martins et al. (2005) for O-type stars. A comparison of the numbers in columns 3–5 of Table 4 shows that, in general, there is good agreement between the effective temperatures derived from FIT*spec* and the values calculated from spectral type and other calibrations. The top plot of Figure 4 compares the effective temperatures obtained from FIT*spec* (triangles) with the spectral type calibrations (asterisks) and the analyses of Martins et al. (2015; plus signs) and Simón-Díaz et al. (2017; squares) for our sample of stars. The error bars measure the uncertainties in $T_{\text{eff}}$ for each star in these calibrations. The largest error bar corresponds to a temperature interval of 1.9 kK, while the shortest one corresponds to a length of 1 kK. The mean absolute errors between the $T_{\text{eff}}$ data derived from FIT*spec* and the corresponding data from spectral type and from all other calibrations in Table 4 are ≈1250 K and ≈2116 K, respectively. If we compare the FIT*spec* data to the more recent calibrations of Nieva (2013), Martins et al. (2015), and Simón-Díaz et al. (2017) the mean absolute error decreases to ≈1880 K. When the uncertainties associated with the FIT*spec* data are neglected, the sample standard deviation is ≈1447 K, which is comparable to the uncertainty of 1000 K in the FIT*spec* data and the mean absolute deviations from the SpT - $T_{\text{eff}}$ and other calibrations in Table 4.

A further important validation of the FIT*spec* code is the comparison of the predicted surface gravities with the literature values. Columns 6–8 of Table 4 provide such a comparison with the SpT–log $g$ calibrations of Martins et al. (2005) and the results from the spectral analyses of Villamariz & Herrero (2002), Nieva (2013), Martins et al. (2015), and Simón-Díaz et al. (2017). There is a general good agreement between the FIT*spec* data and the SpT–log $g$ calibrations. When the uncertainties in the FIT*spec* gravities are neglected, the mean absolute error between both sets of values is ≈0.16 dex. Similarly, the absolute deviation between the FIT*spec* gravities and the values listed in column 8 is ≈0.18 dex, showing good agreement with other calibrations in the literature. The scatter in the FIT*spec* data leads to a sample standard deviation of ≈0.10 dex, which is slightly below the uncertainty of ±0.12 dex in the predicted gravities. The middle plot of Figure 4 shows the comparison of the log $g$ values. The error bars depict the uncertainty in the FIT*spec* values and the calibrations of Martins et al. (2015) (±0.15 dex).

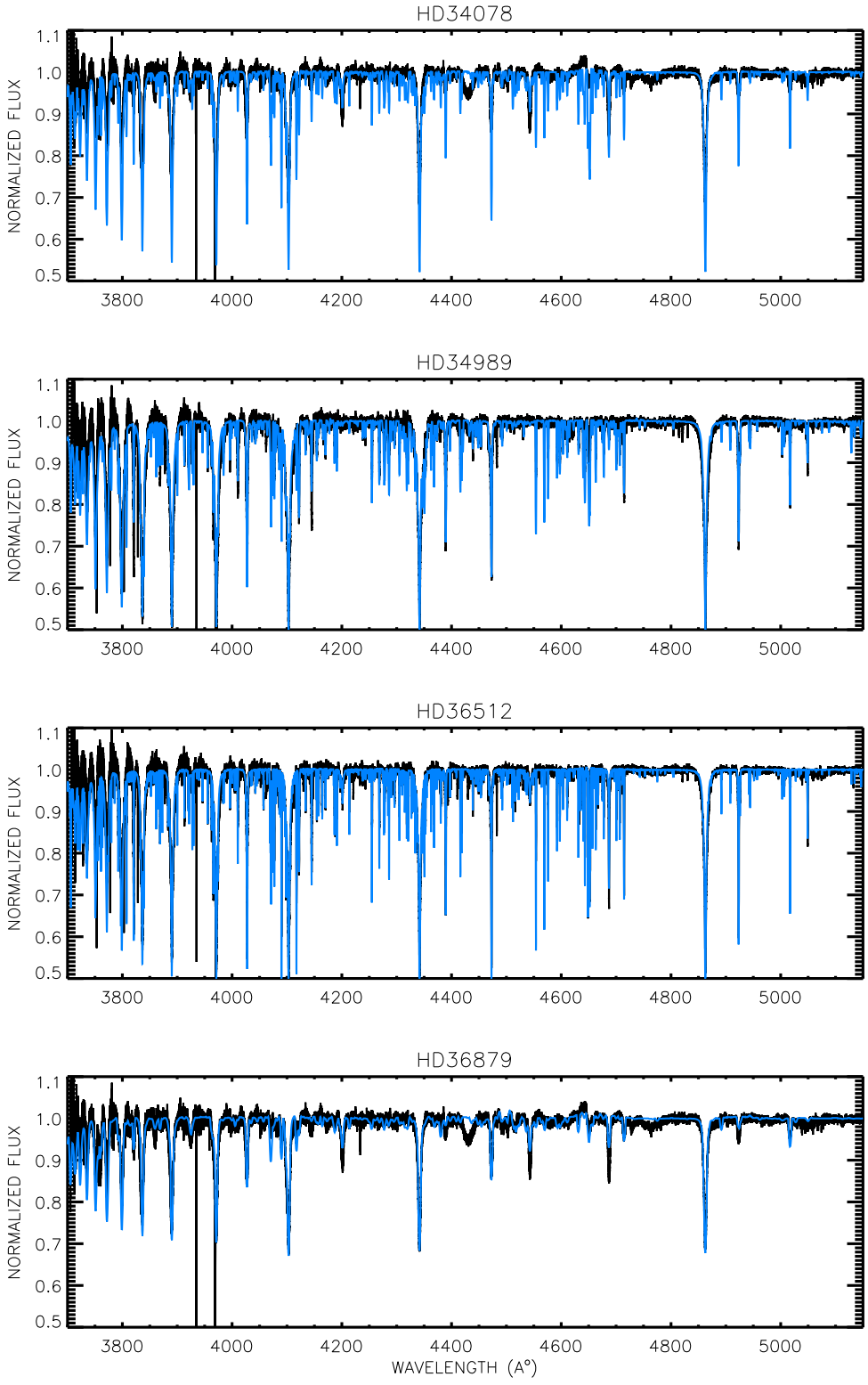


**Figure 6.** Comparison of the observed spectrum (black line) with that of the best-fit model (blue line) for a selected sample of stars.

The luminosities $L$ from spectral type are also calculated using the calibrations of Martins et al. (2005). Columns 9 and 10 of Table 4 compare the luminosities derived from these SpT–$L$ calibrations with those found by FIT*spec*. We may see that the values calculated by FIT*spec* are in very good agreement with those from the spectral type calibrations, with absolute deviations varying from 0.02 to 0.37 dex. This comparison is also displayed in the bottom plot of Figure 4. The uncertainty in the data as represented by the error bars is 0.15 dex for all stars and both calibrations. The mean absolute error between both $\log(L/L_{\odot})$ data sets is ≈0.17 dex, which is very close to the actual uncertainty in the data. The largest deviation from the spectral type luminosities occurs for star HD 53975, with an absolute difference of 0.37 dex. In addition,

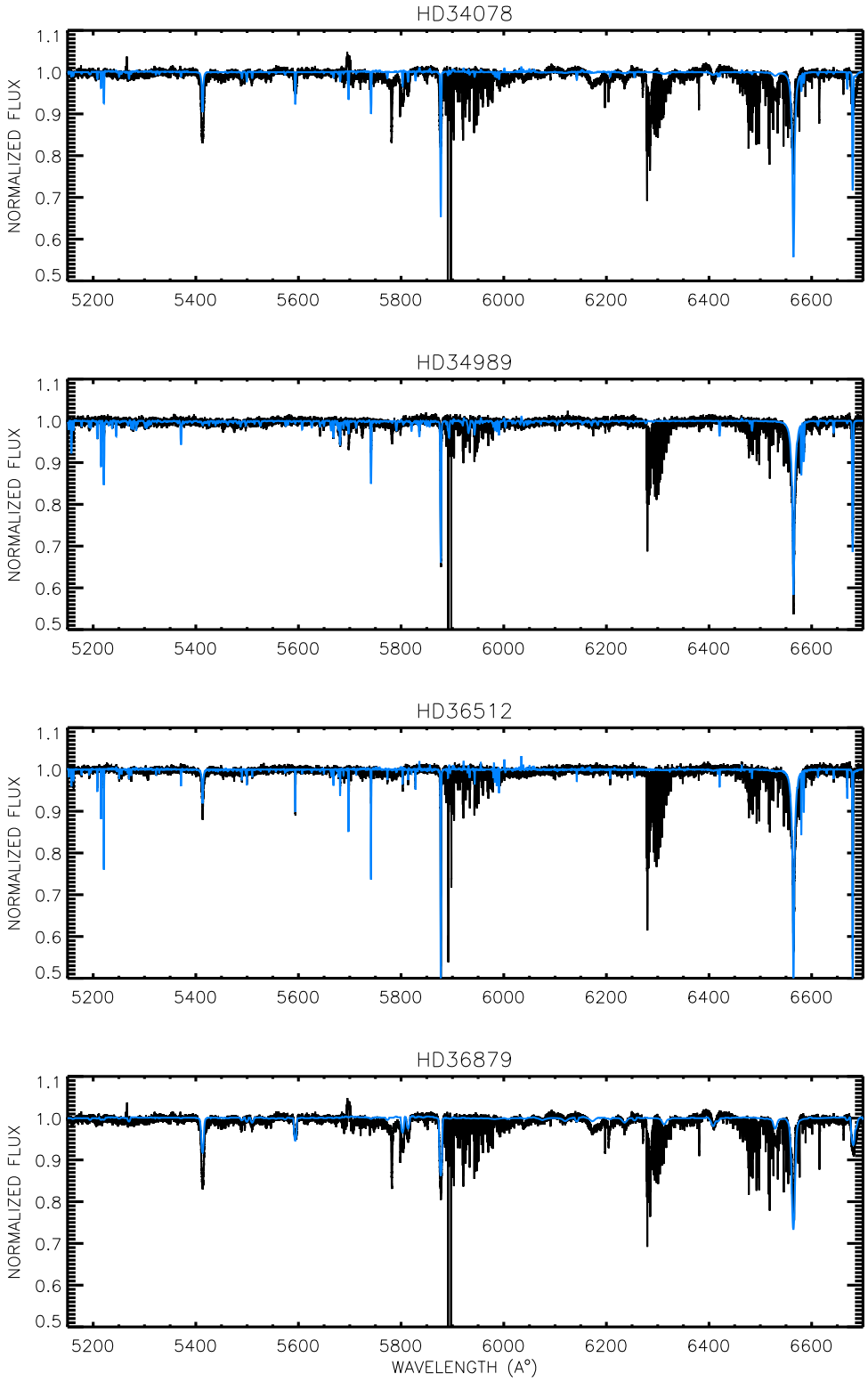


**Figure 7.** Comparison of the observed spectrum (black line) with that of the best-fit model (blue line) for a selected sample of stars.

the luminosities calculated by FIT*spec* exhibit a rather low dispersion with a sample standard deviation of ≈0.168 dex. We note that this value and the mean absolute deviation from the SpT–*L* calibration are barely above the uncertainty in the FIT*spec* luminosities.

It is well-known that the rotational broadening of unblended spectral lines changes the line shape but does not affect the EW of the line (Gray 1992). Therefore, FIT*spec* does not need to apply rotational broadening before the adjustment of the effective temperature and gravity. In fact, this opens the possibility of estimating $v \cdot \sin i$ only with the rotational broadening by adjusting the synthetic spectra to the best fit of the observations, independently of $T_{\rm eff}$ and $\log g$. The last two columns of Table 4 compare the results derived by such

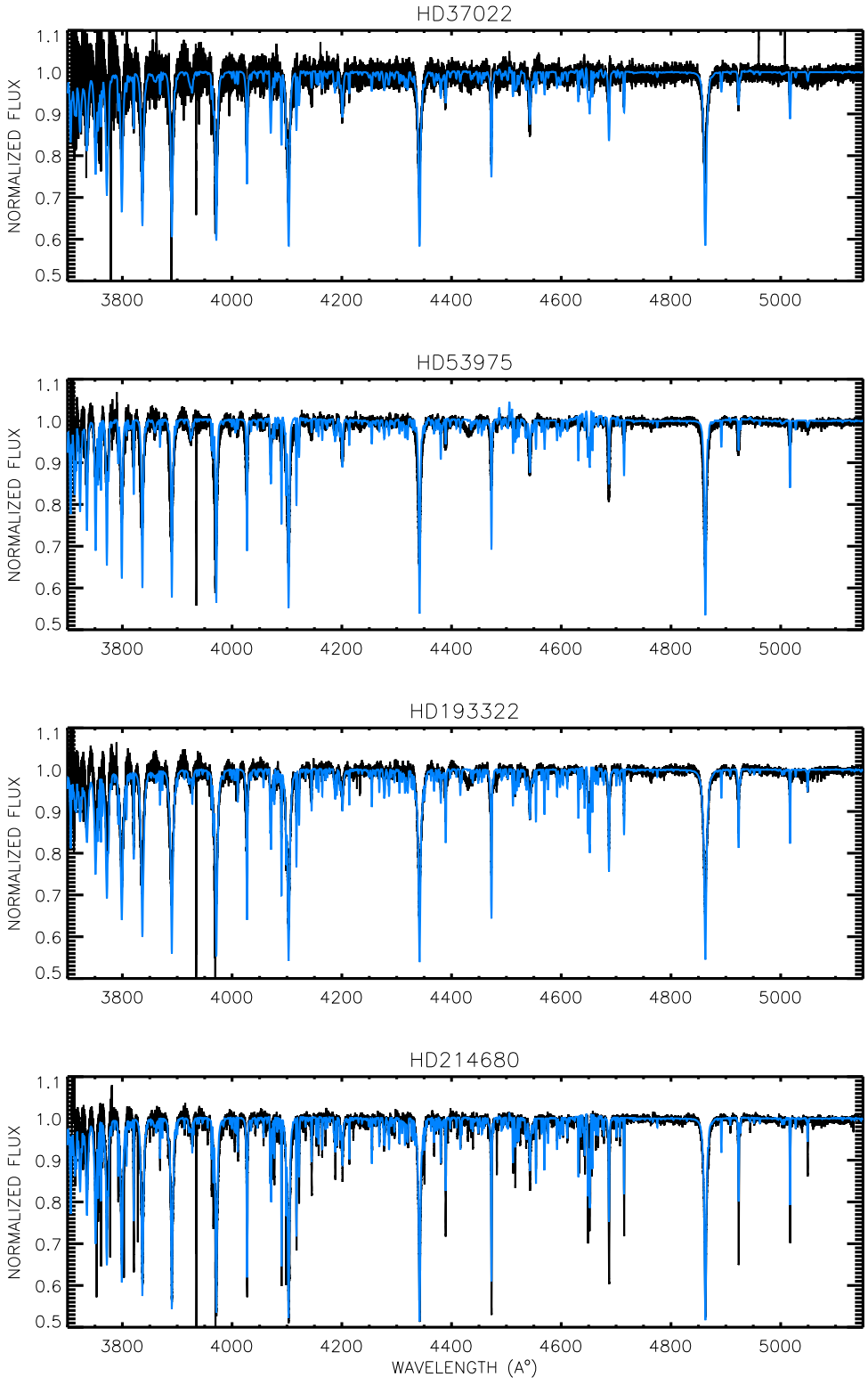


**Figure 8.** Comparison of the observed spectrum (black line) with that of the best-fit model (blue line) for a selected sample of stars.

adjustments with those from several earlier and more recent analyses. The mean absolute errors between both sets of data is $\approx$17.4 km s$^{-1}$. This reasonable agreement demonstrates the reliability of the results for $v \cdot \sin i$. We may see from Table 4 that if the comparison is made with the more recent calibrations of Oliveira & Hébrard (2006), Nieva (2013), Simón-Díaz & Herrero (2014), Martins et al. (2015), and Simón-Díaz et al. (2017), the mean absolute error decreases to $\approx$16.7 km s$^{-1}$. In this work we have not taken into account the contribution of macroturbulence or any other additional broadening mechanism in the determination of the projected rotational velocities. Any additional broadening mechanism will lower the contribution of rotational broadening for a given observation. In particular, Simón-Díaz et al. (2017) used

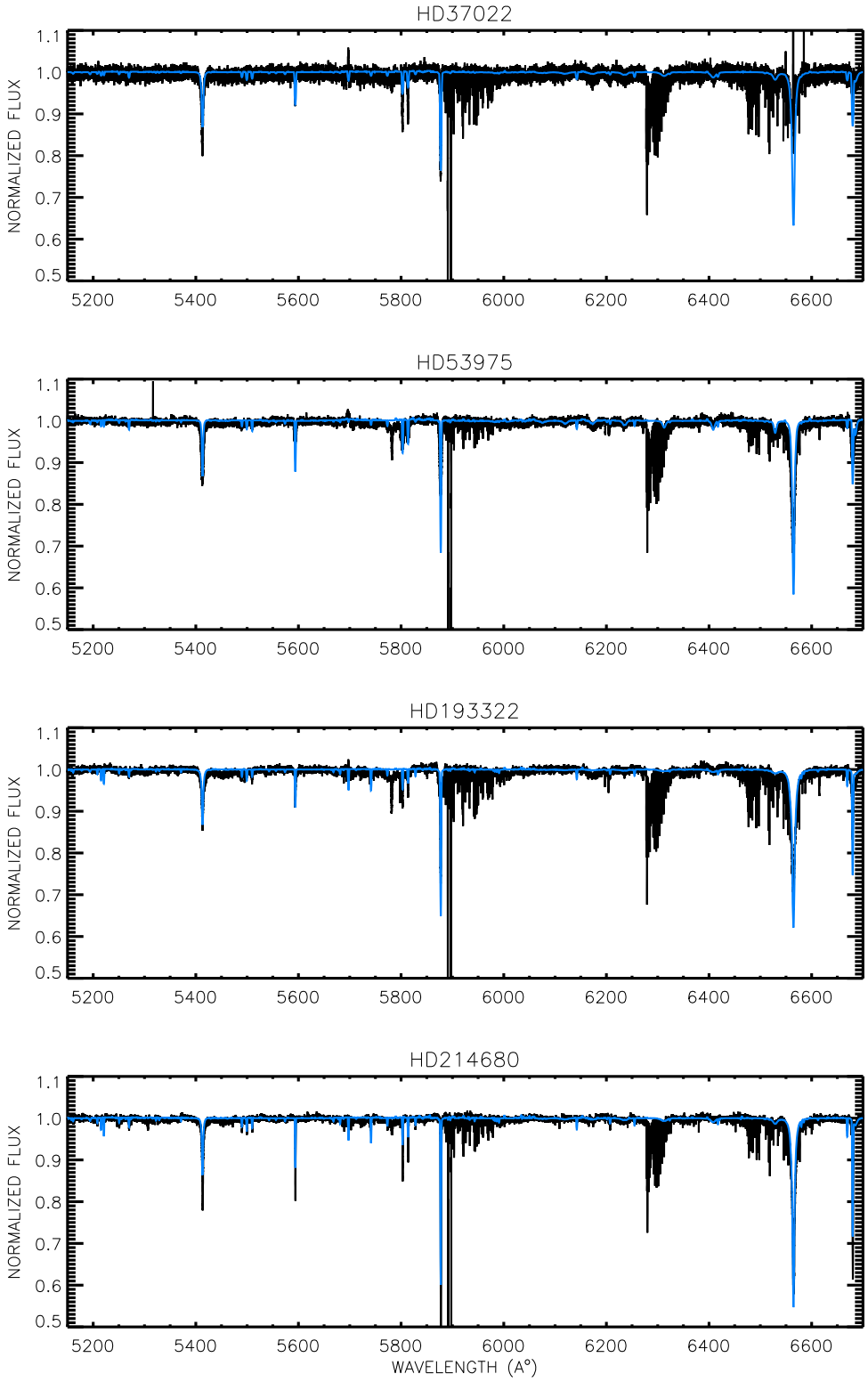


**Figure 9.** Comparison of the observed spectrum (black line) with that of the best-fit model (blue line) for a selected sample of stars.

high-resolution spectra of more than 400 stars with spectral types in the range O4-B9 to provide new empirical clues to explain the occurrence of macroturbulent spectral line-broadening in O- and B-type massive stars. They advanced the hypothesis that macroturbulent broadening may be the result of the combined effects of pulsation modes associated with a heat-driven mechanism and possibly cyclic motions originated by turbulent pressure instabilities, and concluded that the latter mechanism could be mainly responsible of the non-rotational line-broadening detected in OB stars. While the mechanisms proposed by Simón-Díaz et al. (2017) still lack definite confirmation, we may argue, based on the comparison between the results of FIT*spec* and the data of Simón-Díaz et al. (2017) for some of the stars in Table 4, that the effects of

macroturbulent broadening are those of lowering the projected rotational velocities. Finally, Figures 5–9 compare the observed spectrum (black lines) with that derived from the best-fit model (blue lines) for each star of our sample. Most of the salient spectral features are well-reproduced by the models, showing the good quality of the fitting obtained by FIT*spec*. Although the results generated by FIT*spec* are reliable, they can be improved by an expert astronomer. In particular, they can be used in analyses where the parameters of a large number of stars are required to be known or as the starting point to make a better adjustment, especially in calibrations related to the chemical composition of the star. In any case, the use of FIT*spec* represents a considerable saving of time compared to other available tools.

The luminosity of a star is directly related to its mass and gravity, which are directly reflected in the Balmer lines. The depth of these lines is in turn reflected into their equivalent width, which is the main criterion employed by FIT*spec*. The use of this criterion has been demonstrated by the goodness of the fit when comparing the effective temperatures and luminosities with those obtained from SpT–$T_{\rm eff}$ and SpT–$L$ calibrations, respectively. In addition, the synthetic spectra of the 6D grid and the FIT*spec* code can be used to adjust observed spectra from a wide variety of telescopes and spectrographs with different resolutions. A common method for obtaining the best automatic adjustment is to employ chi-squared ($\chi^2$) statistics. However, the appropriate use of a $\chi^2$ test will degrade the synthetic spectra at the resolution of the observation. Considering that the library of synthetic spectra currently consists of 2,835,000 spectra and that it will certainly continue to grow in number, a suitable comparison using the $\chi^2$ statistics involves degrading the synthetic spectra at the same resolution of the observed spectrum. This will also imply the use of additional CPU time. Although this is not a serious problem, it is completely avoided by using the comparison between the EWs and their ratios as the analysis technique. As a final remark, FIT*spec* will soon be available for free download.

## 5. Conclusions

We have developed and tested the FIT*spec* code, which uses a set of modern automatic tools for searching the best-fit models in a database consisting of 27,000 CMFGEN model atmospheres. This database will be soon expanded to 80,000 models. The code performs a quantitative spectroscopic analysis of large samples of O- and B-type stars, using objective criteria in a fast and reliable manner compared to traditional calibration tools. It effectively reduces the time needed for the spectral analysis of massive OB stars from months to hours by identifying those models whose $\mathrm{Error_{tot}}$ is lower than the allowed tolerance of $\lesssim$10% and discarding all those models that do not meet this criterion in order to find the effective temperature ($T_{\rm eff}$) and the surface gravity ($\log g$) of a star by fitting the equivalent widths of optical He and H I Balmer lines.

The reliability of the algorithm was assessed by analyzing the spectra of eight O-type stars taken from the IACOB spectroscopic database of Northern Galactic OB stars and comparing the derived results with those from spectral type–effective temperature (SpT–$T_{\rm eff}$), spectral type–surface gravity (SpT–$\log g$), and spectral type–luminosity (SpT–$L$) calibrations and from previous spectral analysis performed by other authors for the same stars. The values of $T_{\rm eff}$ derived from FIT*spec* are found to match well with those calculated from SpT–$T_{\rm eff}$ calibrations and previous analyses from other authors, with mean absolute errors of $\approx$1250 K and $\approx$2116 K, respectively. The sample standard deviation of the data generated by FIT*spec* is $\approx$1447 K, which is well within the range of the mean absolute deviations from the SpT–$T_{\rm eff}$ and other calibrations in the literature. On the other hand, the values of the surface gravity derived by FIT*spec* agree reasonably well with those obtained from SpT–$\log g$ calibrations, with a mean absolute error of $\approx$0.16 dex. A comparable absolute deviation of $\approx$0.18 dex was obtained by comparing with other calibrations. The values of the stellar luminosity derived by the FIT*spec* algorithm were also found to agree with those obtained from the SpT–$L$ calibrations, with a mean absolute error of $\approx$0.17 dex. This deviation from the SpT–$L$ calibrations is comparable to the uncertainty of 0.15 dex in the FIT*spec* data, which appears to be independent of the spectral type, at least for the stars considered in this study.

In order to complement the database of stellar atmosphere models, we have also developed a library of rotationally broadened synthetic spectra, which allows quick estimation of the projected rotational velocity ($v \cdot \sin i$) of a star. The results of the adjustments using this library are also found to agree reasonably well with results from other spectroscopic analyses for the same stars, with a mean absolute error of $\approx$17.4 km s$^{-1}$ when earlier and recent calibrations are taken into account. If the data are compared only with the more recent calibrations, the mean absolute error is reduced to $\approx$16.7 km s$^{-1}$. The good agreement of the results obtained from FIT*spec* with other spectral analyses demonstrates the reliability of the models.

We thank the referee for providing a number of valuable comments and suggestions that have improved the content of the manuscript. We acknowledge support from the ABACUS-Centro de Matemática Aplicada y Cómputo de Alto Rendimiento of Cinvestav-IPN under grant EDOMEX-2011-C01-165873. J.Z. is grateful for support by the CONACyT project CB-2011-01 No. 168632. The calculations of this paper were performed using the ABACUS computing facilities.

## ORCID iDs

Jaime Klapp https://orcid.org/0000-0003-1828-9183

## References

Asplund, M., Grevesse, N., Sauval, A. J., & Scott, P. 2009, ARA&A, 47, 481
Bouret, J.-C., Lanz, T., Hillier, D. J., et al. 2003, ApJ, 595, 1182
Cassinelli, J. P., & Olson, G. L. 1979, ApJ, 229, 304
Conti, P. S., & Ebbets, D. 1977, ApJ, 213, 438
Crowther, P. A., Hillier, D. J., Evans, C. J., & Fullerton, A. W. 2002, ApJ, 579, 774
Ekström, S., Georgy, C., Eggenberger, P., et al. 2012, A&A, 537, A146
Fierro, C. R., Borissova, J., Zsargó, J., et al. 2015, PASP, 127, 428
Fullerton, A. W. 1990, PhD thesis, Toronto Univ.
Fullerton, A. W., Crowther, P. A., De Marco, O., et al. 2000, ApJL, 538, L43
Gräfener, G., Koesterke, L., & Hamann, W.-R. 2002, A&A, 387, 244
Gray, D. F. 1992, The Observation and Analysis of Stellar Photospheres, Vol. 20
Hamann, W.-R., & Gräfener, G. 2003, A&A, 410, 993
Hamann, W.-R., & Gräfener, G. 2004, A&A, 427, 697
Herald, J. E., & Bianchi, L. 2004, ApJ, 609, 378
Hillier, D. J., Lanz, T., Heap, S. R., et al. 2003, ApJ, 588, 1039
Hillier, D. J., & Miller, D. L. 1998, ApJ, 496, 407
Hubeny, I., & Lanz, T. 1995, ApJ, 439, 875
Krticka, J., & Kubat, J. 2010, A&A, 519, 50
Markova, N., Puls, J., Repolust, T., & Markov, H. 2004, A&A, 413, 693

Martins, F., Hervé, A., Bouret, J. C., et al. 2015, A&A, 575, A34
Martins, F., & Schaerer, D. 2003, in ASP Conf. Ser. 288, Stellar Atmosphere Modeling, ed. I. Hubeny, D. Mihalas, & K. Werner (San Francisco, CA: ASP), 267
Martins, F., Schaerer, D., & Hillier, D. J. 2002, A&A, 382, 999
Martins, F., Schaerer, D., & Hillier, D. J. 2005, A&A, 436, 1049
Mossoux, L., Mahy, L., & Rauw, G. 2018, arXiv:18206535
Nieva, M.-F. 2013, A&A, 550, A26
Oliveira, C. M., & Hébrard, G. 2006, ApJ, 653, 345
Palacios, A., Gebran, M., Josselin, E., et al. 2010, A&A, 516, A13
Puls, J., Urbaneja, M. A., Venero, R., et al. 2005, A&A, 435, 669
Ramachandran, V., Hamann, W.-R., Hainich, R., et al. 2018, arXiv:1802.07494
Sana, H., Le Bouquin, J.-B., Lacour, S., et al. 2014, ApJS, 215, 15
Sander, A., Shenar, T., Hainich, R., et al. 2015, A&A, 577, A13
Santolaya-Rey, A. E., Puls, J., & Herrero, A. 1997, A&A, 323, 488
Simón-Díaz, S., Castro, N., Garcia, M., Herrero, A., & Markova, N. 2011, BSRSL, 80, 514
Simón-Díaz, S., Godart, M., Castro, N., et al. 2017, A&A, 597, A22
Simón-Díaz, S., & Herrero, A. 2014, A&A, 562, A135
Sybesma, C. H. B., & De Loore, C. 1982, A&A, 111, 229
Vacca, W. D., Garmany, C. D., & Shull, J. M. 1996, ApJ, 460, 914
Villamariz, M. R., & Herrero, A. 2002, in ASP Conf. Ser. 274, Observed HR Diagrams and Stellar Evolution, ed. T. Lejeune & J. Fernandez (San Francisco, CA: ASP), 234
Walborn, N. R., & Fitzpatrick, E. L. 1990, PASP, 102, 379
Zsargó, J., Arrieta, A., Fierro, C., et al. 2017, in ASP Conf. Ser. 508, The B[e] Phenomenon: Forty Years of Study, ed. A. Miroshnichenko et al. (San Francisco, CA: ASP), 407